Ultrasonics Sonochemistry 90 (2022) 106164

Contents lists available at ScienceDirect

Ultrasonics Sonochemistry

journal homepage: www.elsevier.com/locate/ultson

Ultrasonically assisted surface modified CeO_2 nanospindle catalysts for conversion of CO_2 and methanol to DMC

Tachatad Kulthananat [a], Pattaraporn Kim-Lohsoontorn [b], Panpailin Seeharaj [a,*]

[a] Advanced Materials Research Unit, Department of Chemistry, School of Science, King Mongkut's Institute of Technology Ladkrabang, Bangkok 10520, Thailand
[b] Center of Excellence on Catalysis and Catalytic Reaction Engineering, Department of Chemical Engineering, Faculty of Engineering, Chulalongkorn University, Bangkok 10330, Thailand

ARTICLE INFO

Keywords:
Surface modification
CeO_2 catalyst
Chemical redox etching
Sonochemistry

ABSTRACT

This study developed a facile and effective approach to engineer the surface properties of cerium oxide (CeO_2) nanospindle catalysts for the direct synthesis of dimethyl carbonate (DMC) from CO_2 and methanol. CeO_2 nanospindles were first prepared by a simple precipitation method followed by wet chemical redox etching with sodium borohydride ($NaBH_4$) under high intensity ultrasonication (ultrasonic horn, 20 kHz, 150 W/cm^2). The ultrasonically assisted surface modification of the CeO_2 nanospindles in $NaBH_4$ led to particle collisions and surface reduction that resulted in an increase in the number of surface-active sites of exposed Ce^{3+} and oxygen vacancies. The surface modified CeO_2 nanospindles showed an improvement of catalytic activity for DMC formation, yielding 17.90 mmol·g_{cat}^{-1} with 100 % DMC selectivity. This study offers a simple and effective method to modify a CeO_2 surface, and it can further be applied for other chemical activities.

1. Introduction

Air pollution is an important cause of the greenhouse effect, which leads to climate change and global warming [1,2]. Carbon dioxide (CO_2), which is emitted upon the combustion of fuels such as natural gas, coal and petroleum from engines and industries [3,4], is reported to be the highest component in the greenhouse gases that are released into the earth's atmosphere [2,3,5]. CO_2 is a stable molecule because it has a linear and centrosymmetric structure [6]. Generally, the transformation of CO_2 into other valuable products requires high energy input as the reactions are thermodynamically unfavorable ($\Delta H = 16.74$ kJ.mol^{-1}) [7]. However, due to it being abundant, inexpensive, non-toxic, non-flammable and renewable [7–9], CO_2 is often used as a starting material in the chemical syntheses of compounds such as methane [10], methanol [11,12], formaldehyde [12], formic acid [10,12], formamides [13], methylamines [13], dimethyl ether (DME) [10,11], and dimethyl carbonate (DMC) [6–9].

DMC is an important organic compound [9,14,15] that is commonly used as an organic solvent and raw material in various chemical industries [7,14,15]. Its favorable biodegradability profile and its low toxicity to humans and the environment have made DMC into a green chemical that is suitable for sustainable production processes [14,16]. There are many applications of DMC including its role as a precursor in the synthesis of polycarbonate and isocyanate [14,17]. DMC can also be used as an electrolyte for lithium-ion batteries, as a fuel additive to increase octane number [18,19], as an intermediate in the synthesis of some antibacterial products, in veterinary drugs [20,21] and in pesticides [22,23]. Recently, the development of a green DMC production route has drawn interest as such a method can simultaneously fulfill industrial demand and tackle an environmental problem [17]. Several routes have been used for the synthesis of DMC, and traditional routes include the phosgene method, oxidative carbonylation, and the transesterification method [9]. In the phosgene method, highly toxic phosgene is used as a starting material and the byproduct, hydrogen chloride (HCl), can cause rapid reactor corrosion [24,25]. In oxidative carbonylation, methanol, oxygen, and carbon monoxide involved in the reaction are toxic and can be explosive [26,27]. Lastly, the transesterification method requires highly toxic chlorobenzene catalysts to catalyze the reaction [28,29]. Compared to these processes, the direct synthesis of DMC from methanol and CO_2 is seen as attractive as it is eco-friendly and produces only water (H_2O) as a byproduct [30–32]. However, due to thermodynamic limitations as shown, $CO_2 + 2CH_3OH \rightarrow (CH_3O)_2CO + H_2O$ ($\Delta G^\circ = 26$ kJ.mol^{-1}), the conversion reaction requires energy input and the DMC yield is relatively low [33–35]. Hence,

* Corresponding author.
E-mail address: panpailin.se@kmitl.ac.th (P. Seeharaj).

https://doi.org/10.1016/j.ultsonch.2022.106164
Received 27 July 2022; Received in revised form 2 September 2022; Accepted 9 September 2022
Available online 13 September 2022

various metal oxide catalysts, for instance, K_2CO_3 [36,37], ZrO_2 [38,39], TiO_2 [40,41] and CeO_2 [19,42–44], have been used to increase the reaction rate and DMC formation.

Cerium oxide (CeO_2) has become the dominant catalyst for the direct synthesis of DMC from CO_2 and methanol due to its high mass density, low thermal expansion, and good physical and chemical stability [45,46]. CeO_2 can shift easily between Ce^{3+} and Ce^{4+}[47], resulting in its rich surface oxygen vacancies and high oxygen storage capacity [48–51]. Although CeO_2 has good catalytic performance in some ways, its catalytic activity in DMC production still needs to be improved [52]. The key factors that affect the catalytic activity of CeO_2 are its morphology and surface properties. Cubic fluorite CeO_2 has various morphologies including different crystal planes and surface properties [53] that can directly affect the interaction between the adsorbed species and the surface-active sites [17,54,55]. Researchers investigated the influence of various morphologies of CeO_2 such as its cubic, rod, sphere, spindle and irregular shapes on catalytic activity. It was found that CeO_2 catalysts with spindle shape morphology showed better catalytic performance in the direct synthesis of DMC from CO_2 and methanol [8,17,34]. The excellent catalytic activity of CeO_2 nanospindle catalysts in the formation of DMC was suggested to be because the surface of each cubic fluorite CeO_2 spindle consisted of an active exposed (1 1 1) plane that had a large number of surface defect sites that could activate CO_2 and methanol, and also had a high potential to absorb CO_2 [8,17,48].

The catalytic activity of CeO_2 can also be improved by engineering its surface. The surface properties play a critical role in catalyst dispersion, stabilization and reactive gas adsorption–desorption [56–58]. The CeO_2 surface can be modified by increasing the number of surface active sites by varying specific surface areas, pore sites, the ratio of Ce^{3+}/Ce^{4+}, and the number of oxygen vacancies and acid-base sites [59]. There are many processes that can be used for modifying a CeO_2 surface, such as annealing under vacuum [60], hydrogen treatment [61], thermal activation [62], thermal annealing treatment [35,63], electron beam irradiation [64], and pressure control [65]. However, these processes are difficult to control and require expensive equipment and tools. Wet chemical redox etching is an interesting process for modifying a CeO_2 surface because it is a simple, inexpensive and effective process [66–69]. Chemical redox etching of CeO_2 nanorods with reducing agents such as sodium borohydride ($NaBH_4$) [66,68,69], ascorbic acid and hydrogen peroxide (H_2O_2) [67] produced superior catalytic activity in low temperature CO oxidation due to the formation of porous and rough surfaces, and an increase in specific surface areas, surface Ce^{3+} fractions and concentration of oxygen vacancies [66–69]. The catalytic activity of CeO_2 in the CO oxidation reaction can further be improved after the chemical redox etching process by impregnation with active metals or metal oxides such as Pt [57], Ru [68], CuO_x [4,66,70], CoO_x, NiO_x, FeO_x, and MnO_x [66]. These two-step treatments can effectively improve the dispersion of the impregnated species and also prevent the migration and aggregation of these active species on the surface of CeO_2. Wang et al. [66] reported that impregnation of CeO_2 nanorods with CuO after wet chemical redox etching with $NaBH_4$ to form CeO_2-CuO catalysts could enhance the catalytic activity for low temperature CO oxidation reaction due to the strong interfacial interaction between Cu ions and Ce ions resulting in the formation of surface-active sites through the oxidation–reduction reaction of $Cu^+ + Ce^{4+} \leftrightarrow Cu^{2+} + Ce^{3+}$. The surface modification of CeO_2 catalysts by wet chemical redox etching has been reported to be a simple and effective route for improving the catalytic activity. Furthermore, this interesting approach has not yet been applied and investigated in the modification of spindle shape CeO_2 catalysts for the direct synthesis of DMC from CO_2 and methanol. Therefore, in this work, we proposed a new strategy to engineer the surface properties of CeO_2 nanospindle catalysts using wet chemical redox etching process followed by incorporation of CuO active species by a wet impregnation process. Moreover, the treatment processes were improved using sono-assisted ultrasonication, in which the medium solution was irradiated with a high intensity ultrasonic waves of frequency 20 kHz–15 MHz and acoustic wavelength of 100 mm-100 μm to increase the surface reaction between CeO_2 nanospindles and the treatment reagents [71–73]. Finally, the characterization and investigation of the catalytic performance for the direct synthesis of DMC from CO_2 and methanol of these surface modified CeO_2 nanospindles was reported.

2. Material and methods

2.1. Synthesis of cerium oxide (CeO_2) nanospindles

CeO_2 was synthesized via a precipitation method. Firstly, 12 mmol of cerium(III) nitrate hexahydrate ($Ce(NO_3)_3{\cdot}6H_2O$; purity 99.5 %, Carlo Erba) and 400 mmol of urea ($CO(NH_2)_2$; purity 99.0 %, Carlo Erba) were dissolved in 300 ml distilled water. The solution was ultrasonically irradiated with a low intensity ultrasonic wave (37 kHz, 80 W) in an ultrasonic bath at 70 °C for 1 h to obtain a white suspension. Next, the suspension was refluxed at 95 °C for 2 h in a round bottomed flask under magnetic stirring. After the reaction finished, the precipitates were centrifugally separated, dried overnight at 80 °C, and finally calcined in ambient air at 650 °C for 2 h.

2.2. Surface modification of CeO_2 nanospindles

The obtained CeO_2 nanospindles was chemically treated to modify their surface with a reducing agent, sodium borohydride ($NaBH_4$; purity 98.0 %, Acros organics) and copper(II) nitrate trihydrate ($Cu(NO_3)_2{\cdot}3H_2O$; purity 99.0 %, Carlo Erba) with the assistance of a high intensity ultrasonic wave. Firstly, 1.000x g of CeO_2 was dispersed in 194 ml distilled water in a sonochemical reaction vessel. The suspension was then ultrasonically irradiated with a high intensity ultrasonic wave (Ti-horn, 20 kHz, 150 W/cm^2 Sonics Model VCX 750, Vibracell) for 2 min. Next, 6 ml of 4 M $NaBH_4$ or 5 wt% of $Cu(NO_3)_2{\cdot}3H_2O$ was added and the suspensions were continuously irradiated until the 30 min mark. After that the products were centrifugally separated, dried overnight at 80 °C, and finally calcined in air at 400 °C for 2 h to create a strong interaction between B- species and CeO_2 surface and to convert Cu- species into oxide form. The catalysts after chemical treatment with $NaBH_4$ and $Cu(NO_3)_2{\cdot}3H_2O$ were labeled as CeO_2-B and CeO_2-CuO, respectively. CeO_2-H_2O catalyst was prepared via the same procedure except that the CeO_2 was treated in de-ionized water under a high intensity ultrasonication. The CeO_2-B-CuO catalyst was chemically treated in two-step with 4 M $NaBH_4$, followed by 5 wt% of $Cu(NO_3)_2{\cdot}3H_2O$ and after the treatment processes, the products were calcined only once at 400 °C for 2 h. Notably, $NaBH_4$ was chosen as a reducing agent in the work as it is a strong and effective reducing agent that is commonly used in laboratory and industrial applications.

2.3. Characterization

Catalyst morphology was determined by scanning electron microscope (SEM; FEI Quanta 250, samples preparation with gold (Au) coating) and transmission electron microscope (TEM; FEI Tecnai G2 20). Elemental composition was investigated with an energy-dispersive spectroscope (EDS, Oxford Instrument X-max 20) equipped with SEM. The particle size was estimated by measuring the size of at least 50 particles in SEM images using the ImageJ program. The powder X-ray diffraction (XRD) patterns were recorded on a Rigaku Smartlab diffractometer with a CuKα (40 kV, 30 mA) radiation at the diffraction angle (2θ) range of 5–90° with a scanning rate of 20.00° min^{-1} and indexing from the JCPDS (ICDD) database. Debye-Scherrer's equation shown in Eq. (1) was used for calculation of the crystallite size (D) from XRD data [74]:

$$D = \frac{k\lambda}{\beta_{hkl}\cos\theta} \quad (1)$$

where k is a constant taken as 0.94, λ is X-ray wavelength (CuKα radiation 0.15418 nm), β_{hkl} is the full width at half maximum (FWHM) of intensity of the diffraction peak, *hkl* are the Miller indices of the planes being analyzed, and θ is the diffraction angle. The lattice constant (a) was calculated from the Bragg equation and the crystal spacing formula as shown in Eq. (2) and Eq. (3) [52,73]:

$$2d\sin\theta = n\lambda \tag{2}$$

$$d_{hkl} = \frac{a}{\sqrt{h^2 + k^2 + l^2}} \tag{3}$$

where n is the reflection series and d_{hkl} is the crystal spacing. Molecular structure of the catalysts was analyzed using a Fourier transform infrared spectrometer (FT-IR; Perkin Elmer, Spectrum Gx) and Raman spectrometer (Thermo Scientific, DXR Smart, 532 nm excitation solid state laser in the range of 200–1500 cm^{-1}). The Brunauer-Emmett-Teller (BET) specific surface area was tested by nitrogen adsorption–desorption with Autosorb (Autosorb 1). X-ray photoelectron spectroscopy (XPS; Kratos, Amicus with MgKα anode 20 mA and 10 kV) was employed to estimate the surface states of elemental composition by Gaussian fitting the XPS spectra using MagicPolt program. Ammonia (NH_3) and carbon dioxide (CO_2) temperature programmed desorption (TPD; Carbolite) was used to characterize acid-base properties of the catalysts. The samples were saturated with pure NH_3 or CO_2 at 50 °C, then purged with Argon (Ar) under a flow rate of 30 $ml.min^{-1}$ for 30 min to remove the physisorbed NH_3 or CO_2 and finally heated to 950 °C under a constant helium (He) flow rate of 30 ml min^{-1} to determine concentration of NH_3 or CO_2 desorption.

2.4. Catalytic activity test for the direct synthesis of DMC from CO_2 and methanol

100 mg of each of the prepared catalyst powders and 40 ml of liquid methanol (CH_3OH; purity 99.8 %, RCI Labscan) were charged into a 250 ml stainless-steel autoclave reactor equipped with a stirrer. The reactor was sealed and subsequently pressurized up to 4.5 MPa with CO_2 gas (purity 99.8 %, Linde). The reaction was conducted at 140 °C for 3 h under constant stirring at 400 rpm. After the reaction had finished, the reactor was cooled down to room temperature and this was followed by depressurizing. Each catalyst was then separated from the liquid products. The products were analyzed by gas chromatography (GC; Shimadzu, Nexis GC 2030) with a capillary column (SH-RTX-624, 30 m × 0.25 mm, film thickness 1.40 μm). The column temperature program chosen was as follows: 50 °C for 4 min, then increase to 240 °C at a rate of 10 °C min^{-1}. Helium (He; purity 99.8 % Linde) was used as the carrier gas with a flow rate of 1.88 ml min^{-1}. The products were determined using a flame ionization detector (FID). Dimethyl carbonate in methanol was added as a standard substance to quantitatively analyze the products using the calibration curve method. Finally, the DMC yield (mmol. g_{cat}^{-1}), the CH_3OH conversion (%) and the turnover frequency (TOF, h^{-1}) were determined from the amount of initial catalyst (0.1 g), methanol (40 ml) usage, and the DMC product formation and reaction times, respectively, using Eq. (4) – Eq. (6), as follows [75–77]:

$$\text{DMC yield}\,(\text{mmol}.g_{cat}^{-1}) = \frac{\text{DMC}\,(\text{mmol})}{\text{Catalyst}\,(\text{g})} \tag{4}$$

$$CH_3OH\,\text{conversion}\,(\%) = \frac{\text{DMC}\,(\text{mol}) \times 2}{CH_3OH\,(\text{mol})} \times 100\,\% \tag{5}$$

$$\text{TOF}\,(h^{-1}) = \frac{\text{DMC}\,(\text{g})}{\text{Catalyst}\,(\text{g}) \times \text{reaction time}\,(\text{h})} \tag{6}$$

The DMC selectivity (%) was estimated from the amount of DMC formation to the amount of total liquid products except for the remaining methanol and water by product using Eq. (7) [76]:

$$\text{DMC selectivity}\,(\%) = \frac{\text{DMC}}{\text{DMC} + \text{by product}} \times 100\% \tag{7}$$

3. Results and discussion

3.1. Catalyst characterization

The XRD patterns of CeO_2 and surface modified CeO_2 catalysts with de-ionized water (CeO_2-H_2O), $NaBH_4$ (CeO_2-B), CuO (CeO_2-CuO) and two-step treatment with $NaBH_4$ followed by CuO (CeO_2-B-CuO) under high intensity ultrasonic irradiation are illustrated in Fig. 1. All catalyst peaks were indexed to the face centered cubic CeO_2 of fluorite structure (JCPDS 00–034-0394, space group *Fm3m* (225)) [17,52]. All catalysts had good crystallinity, demonstrating that modification with $NaBH_4$ and/or CuO had not altered the original fluorite-type structure of CeO_2. There was no diffraction peak related to B- and Cu- phases observed in the XRD patterns of CeO_2-B, CeO_2-CuO and CeO_2-B-CuO catalysts and this was probably because only low concentrations of B- and Cu- species existed in the CeO_2 based catalysts. The calculated lattice parameters and crystallite sizes using the Debye Scherrer equation [74] of all catalysts are shown in Table 1. The lattice parameter and crystallite size of unmodified CeO_2 were 5.4165 ± 0.0022 Å and 19.36 ± 3.28 nm, respectively. After the surface modification, the lattice parameter and crystallite size tended to decrease, varying between 5.4109 and 5.4121 Å and 16.81–19.56 nm. The decrease of both lattice parameter and crystallite size after modification of the CeO_2 surface could have been related to the formation of surface defects caused by two major factors, firstly, the collision of catalyst particles due to an acoustic cavitation stimulated by high intensity ultrasonic irradiation [78–82] and secondly, the reduction of Ce^{4+} to Ce^{3+} due to the redox reaction of CeO_2 surface with $NaBH_4$ reducing agent and Cu-species, which consequently led to the formation of oxygen vacancies to maintain charge neutrality in the ionic structure [31,52,66]. Even though Ce^{3+} has a slightly larger ionic radius than Ce^{4+} (ionic radius with 8-fold coordination of Ce^{3+} = 1.143 Å and Ce^{4+} = 0.97 Å), the increase of surface oxygen vacancy concentration seemed to have a bigger effect as it decreased the effective anionic radius in the fluorite lattice, which resulted in the variation of the lattice parameter [81,83].

The FT-IR spectra of the CeO_2 and surface modified CeO_2 catalysts in the range of 400–4000 cm^{-1} are shown in Fig. 2. The spectra of all catalysts showed the characteristic absorption bands of Ce-O stretching vibration at 565 cm^{-1} [84]. The complex bands observed at 1300 and 1050 cm^{-1} correlated with the adsorption of carbonate species (CO_3^-) on the surface, which might have formed during the preparation process

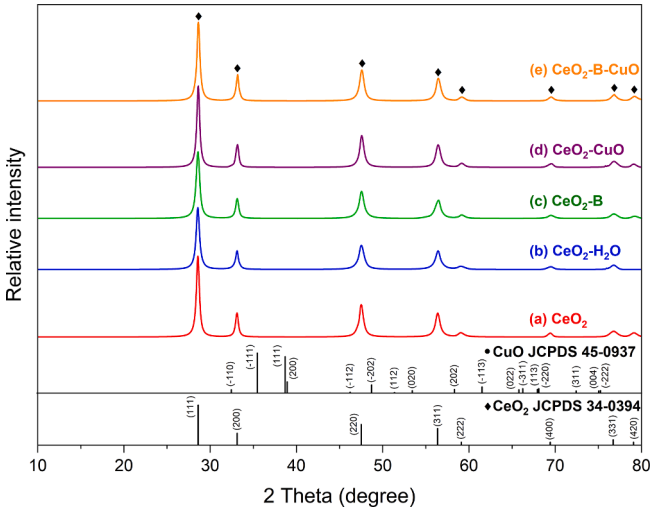

Fig. 1. XRD patterns of CeO_2 and surface modified CeO_2.

Table 1
Crystal properties, particle size and surface area of CeO_2 and surface modified CeO_2.

Catalyst	Lattice parameter (Å)	Crystallite size (nm)	Particle size (μm)		Surface area (m^2g^{-1})
			Width	Length	
CeO_2	5.4165 ± 0.0022	19.36 ± 3.28	1.38 ± 0.42	5.53 ± 1.42	65.56
CeO_2-H_2O	5.4121 ± 0.0030	17.39 ± 4.66	1.16 ± 0.54	4.98 ± 1.66	75.21
CeO_2-B	5.4113 ± 0.0048	16.81 ± 3.62	0.81 ± 0.15	4.24 ± 0.61	70.17
CeO_2-CuO	5.4109 ± 0.0025	19.07 ± 3.81	1.08 ± 0.38	4.94 ± 1.67	79.32
CeO_2-B-CuO	5.4118 ± 0.0036	19.56 ± 4.96	1.21 ± 0.36	5.07 ± 1.26	50.50

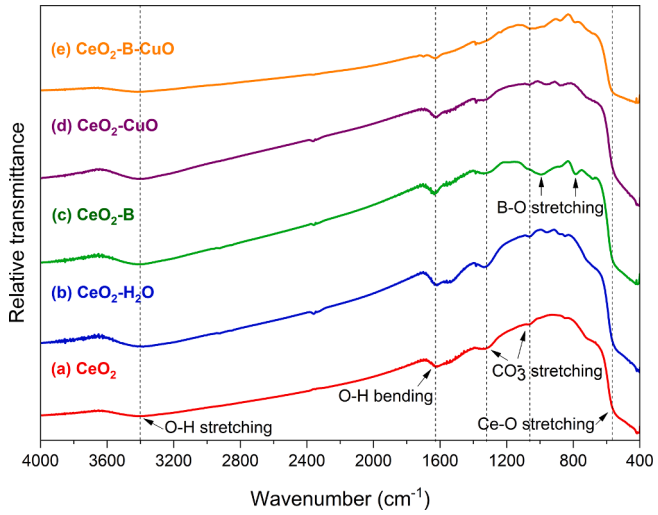

Fig. 2. FTIR spectra of CeO_2 and surface modified CeO_2.

and storage [85–87]. The absorption bands of the hydroxyl (O—H) groups of physisorbed water appeared around 3400 cm^{-1} for the O—H stretching vibration and at 1630 cm^{-1} for the scissor bending vibration [84,88–90]. It is interesting to note that the intensity of the absorption bands related to the CO_3^- and O—H groups of the surface modified CeO_2 catalysts, especially in the case of CeO_2-H_2O, increased when compared with those of unmodified CeO_2, and this could have been because there had been an increase in the number of surface-active sites that absorbed foreign species after surface modification under a high intensity ultrasonic irradiation. In the case of the CeO_2-B and CeO_2-B-CuO catalysts, the absorption bands of B-O asymmetric and symmetric stretching vibrations were also observed at 988 and 798 cm^{-1}, respectively [91–93], indicating the presence of B-species in these catalysts.

The morphology of the catalysts was investigated by SEM and TEM, and the results are shown in Figs. 3 and 4, respectively. The average particle sizes obtained by measuring width at center and length of catalyst particles observed in the SEM images are summarized in Table 1. Before the surface modification (Figs. 3(a) and 4(a)), CeO_2 consisted in spindle-shaped particles with width at center of 1.38 ± 0.42 μm and length of 5.53 ± 1.42 μm. The edges of the spindles were curved, and the ends were pointy, indicating the existence of defect sites [17]. The results from the XRD and SEM study confirmed that the CeO_2 nanospindles had simply been prepared via a precipitation method. After the surface modification with H_2O, $NaBH_4$ and CuO under high intensity ultrasonic irradiation, significant changes on the catalyst surface, such as surface roughness or pore formation, could not be seen clearly in the SEM (Fig. 3(b)–(e)) and TEM images (Fig. 4(b)). However, some imperfect spindles and debris were observed in SEM images of the surface modified catalysts CeO_2-H_2O, CeO_2-B, CeO_2-CuO and CeO_2-B-CuO (Fig. 3(b)–(e)). Particle collision induced by acoustic cavitation (the formation, growth, and collapse of microbubbles) created a microjet effect which led to particle breakage [78–80,94] and thus resulted in the decrease of average particle size, as shown in Table 1.

The SEM image, EDS spectrum and elemental mapping of the two-step treatment CeO_2-B-CuO catalyst are presented in Fig. 5. The EDS spectrum confirmed that the CeO_2-B-CuO catalyst consisted of Ce, O, B and Cu elements. The elemental mappings showed that the B- and Cu-species were uniformly dispersed throughout the CeO_2 phase. As in the preparation processes, the surface modified CeO_2 catalysts were calcined in air at 400 °C for 2 h after the chemical treatment with $NaBH_4$ and $Cu(NO_3)_2{\cdot}3H_2O$, so the B- and Cu- species were more likely to exist as nanocrystalline B_2O_3 and CuO on CeO_2 surface.

The specific surface areas of catalysts obtained through nitrogen adsorption–desorption measurements are shown in Table 1. The surface area of CeO_2 nanospindles was 65.56 m^2g^{-1}, and it increased to 75.21 m^2g^{-1} (CeO_2-H_2O), 70.17 m^2g^{-1} (CeO_2-B) and 79.32 m^2g^{-1} (CeO_2-CuO) after the surface modification. The increase of surface area after the surface modification agreed well with the reduction of particle size caused by particle collisions stimulated by high intensity ultrasonic irradiation. In case of the CeO_2-CuO catalyst, the highest specific surface at 79.32 m^2g^{-1} could have presented due to the contribution of the high specific surface area phase of nanocrystalline CuO. In the case of the CeO_2-B-CuO catalyst, the surface area had decreased to 50.50 m^2g^{-1}. This may have been due to redox etching agent $NaBH_4$ creating defect sites on the surface of CeO_2, which led to strong interfacial bonding between the defect sites and nanocrystalline CuO, thus resulting in the decrease of specific surface area of the CeO_2-B-CuO catalyst [57,66,95,96].

Raman spectroscopy was performed to study the defects in the catalyst structures. The Raman spectra of CeO_2 and surface modified CeO_2 nanospindle catalysts (Fig. 6) showed the characteristic Raman active bands of CeO_2 at ~ 464 cm^{-1}, typical of the triply degenerate F_{2g} vibrational modes of fluorite-type structures [52]. The weak bands around 255 and 600 cm^{-1} were assigned to the double degenerate TO mode (2TA) and the defect-induced band (D band), respectively [52,66]. The Raman active bands related to peroxide species (O_2^{2-}) were also observed around 831 cm^{-1} [66] and the intensity of these bands tended to decrease after the surface modification. When considered the characteristic F_{2g} bands, the band intensities were found to decrease after the surface modification and the Raman shift of these F_{2g} bands was 464, 463, 462, 457 and 456 cm^{-1} for CeO_2, CeO_2-H_2O, CeO_2-B, CeO_2-CuO and CeO_2-B-CuO, respectively, indicative of red shift after the surface modification. The decrease of the F_{2g} band intensity and Raman shift position after the surface modification could be attributed to the variation of Ce-O bond length in the fluorite crystal due to a partial reduction of the smaller ionic radius Ce^{4+} cations to larger Ce^{3+} cations [52,97,98], as well as the decrease of crystallite site caused by the formation of defect sites on the CeO_2 surface [52,67]. The results of the Raman study were consistent with the change in crystal lattice as observed in the XRD analysis.

The surface states of CeO_2 and surface modified CeO_2 nanospindle catalysts were further analyzed using the XPS technique. The Ce 3d spectra, each composed of 10 peaks, are shown in Fig. 7. The 10 peaks were assigned as V and U, corresponding to the spin–orbit multiplets of Ce $3d_{5/2}$ and Ce $3d_{3/2}$, respectively [52,99]. The peaks V^0 (881.18 eV), V' (886.78 eV), U^0 (900.38 eV), and U' (904.44 eV) belonged to the Ce^{3+} state, while the peaks V (883.47 eV), V'' (890.37 eV), V''' (898.69 eV), U (902 eV), U'' (907.94 eV), and U''' (917.47 eV) belonged to the Ce^{4+} state [66]. The O 1 s spectra for all catalysts are illustrated in Fig. 8. In the literature, three types of peaks in the integral fitting of the O 1s spectrum were commonly ascribed to three oxygen species: lattice oxygen (O_L), oxygen vacancy (O_V), and surface-chemisorbed oxygen species or oxygen in hydroxyl groups (O_C). The peaks at 529.7, 531, and 532.5 eV were assigned to O_L, O_V, and O_C on the catalyst surface,

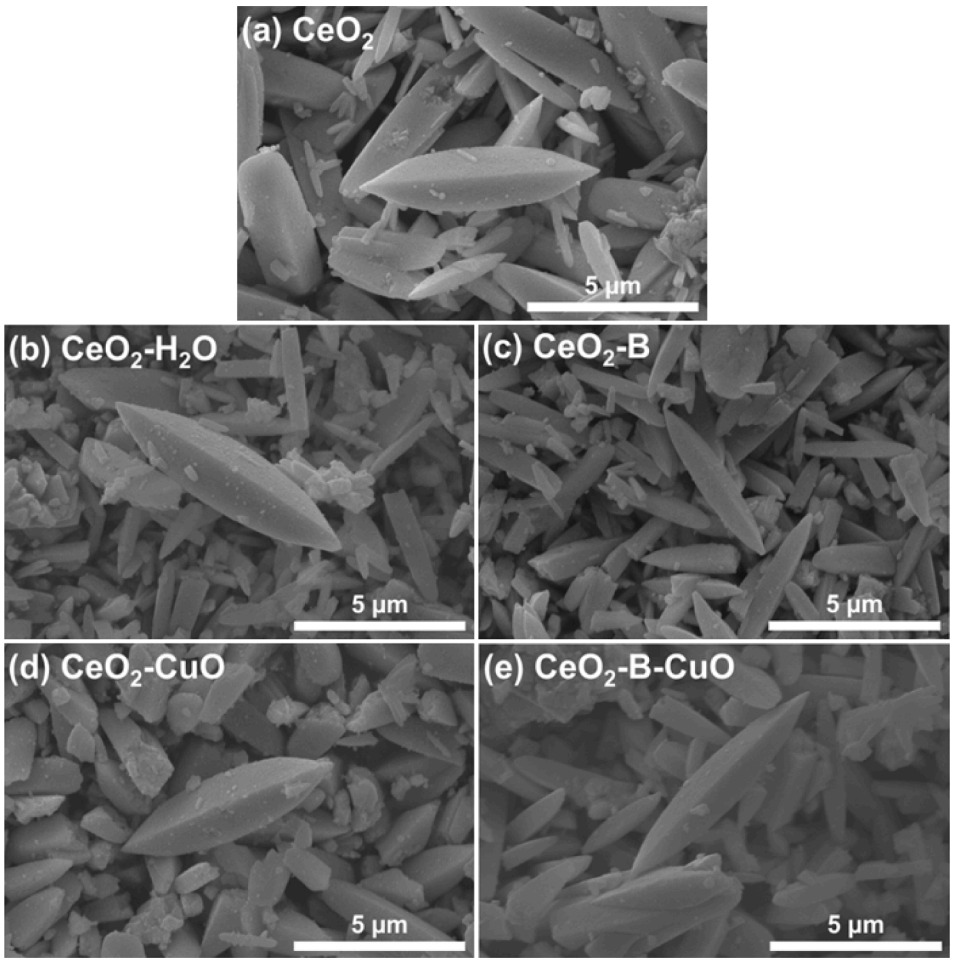

Fig. 3. SEM images of (a) CeO_2, (b) CeO_2-H_2O, (c) CeO_2-B, (d) CeO_2-CuO and (e) CeO_2-B-CuO.

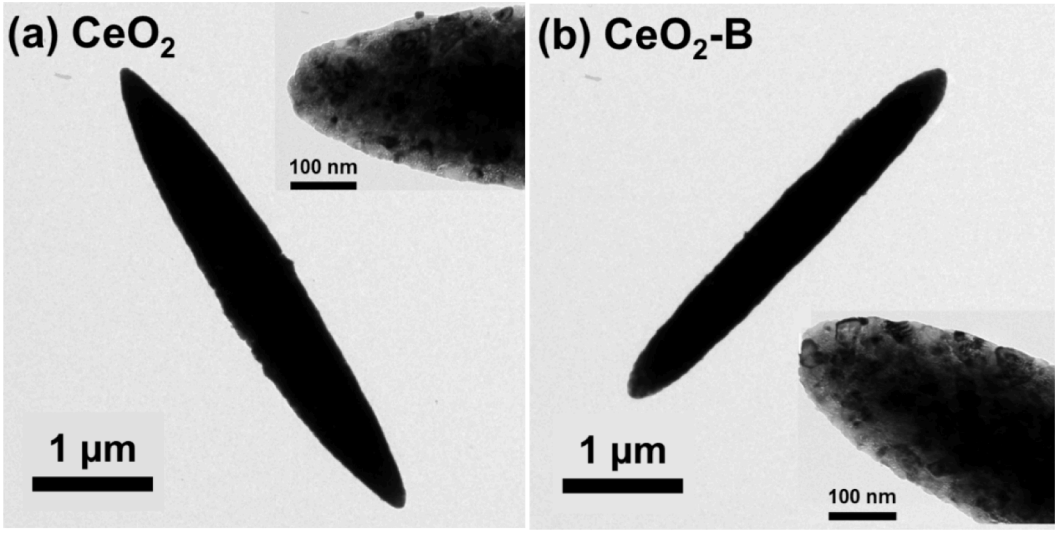

Fig. 4. TEM images of (a) CeO_2 and (b) CeO_2-B.

respectively [66]. For the CeO_2-B catalyst, the O_C peak appeared slightly shifted to higher binding energy, and this could indicate the presence of another oxygen type of B-O which was typically observed at 533.2 eV [100]. In case of CeO_2-CuO and CeO_2-B-CuO, the O_L peaks slightly had shifted to lower binding energy. A possible reason for the shift of the O_L peaks could have been the contribution from the $O_L(Cu^{2+})$ of CuO phase, which was generally observed at 529 eV [101].

The quantitative assessment of the surface concentrations of Ce^{3+} ($[Ce^{3+}]$) and Ce^{4+} ($[Ce^{4+}]$) in the total Ce content was estimated from the total integrated areas of the Gaussian fitting peaks using Eq. (7) and Eq. (8) [102]. The proportion of O_V to the total surface oxygen species ($[O_V]$) was estimated using Eq. (9) [103]:

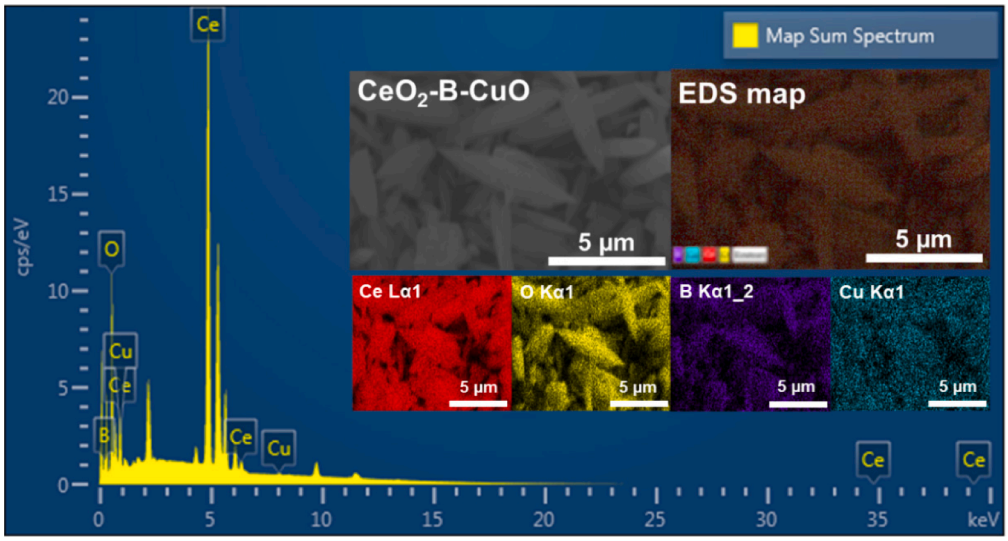

Fig. 5. EDS spetrum, SEM image and elemental mapping of CeO_2-B-CuO.

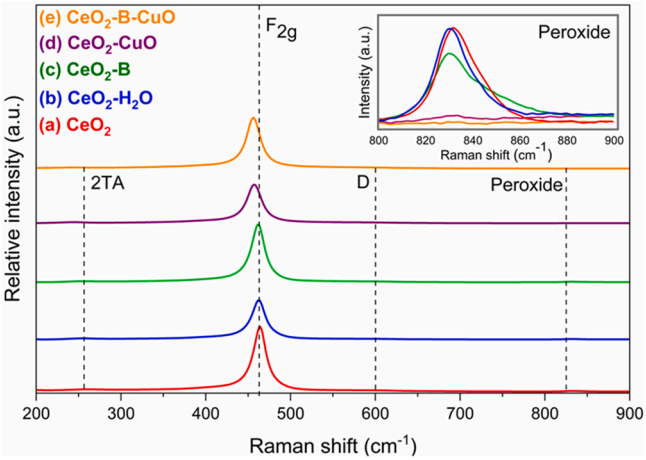

Fig. 6. Raman spectra of CeO_2 and surface modified CeO_2.

$$[Ce^{3+}](\%) = \frac{U^0 + U' + V^0 + V'}{(U + U'' + U''' + V + V'' + V''') + (U^0 + U' + V^0 + V')} x100\% \quad (7)$$

$$[Ce^{4+}](\%) = \frac{U + U'' + U''' + V + V'' + V'''}{(U + U'' + U''' + V + V'' + V''') + (U^0 + U' + V^0 + V')} x100\% \quad (8)$$

$$[O_V](\%) = \frac{O_V}{(O_V + O_L + O_C)} x100 \quad (9)$$

The surface concentration fractions of Ce^{3+}, Ce^{4+} and Ov on the CeO_2 and surface modified CeO_2 catalysts are shown in Table 2. The $[Ce^{3+}]$ of CeO_2 nanospindles was 9.06 %, and it increased to 9.61 %, 14.03 %, 10.16 % and 10.71 % for CeO_2-H_2O, CeO_2-B, CeO_2-CuO and CeO_2-B-CuO, respectively. The increase of $[Ce^{3+}]$ was consistent with changes in oxygen vacancy concentration, $[O_v]$, from 20.81 % to 26.37–48.70 % after the surface modification since the reduction of Ce^{4+} to Ce^{3+} species resulted in the generation of oxygen vacancies to manage charge balance [99,104]. The increase of defect sites after the surface modification was due to the synergistic effects of the increase of surface-active area caused by particle collisions induced by the high intensity ultrasonic irradiation together with the reduction of Ce^{4+} to

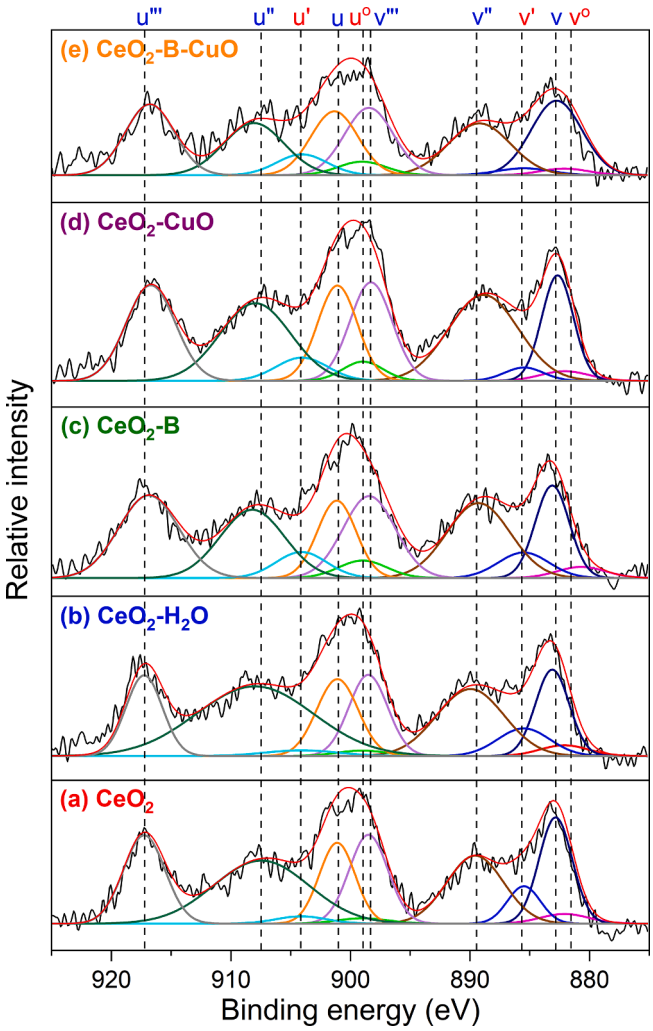

Fig. 7. XPS spectra of Ce 3d of CeO_2 and surface modified CeO_2.

Ce^{3+} from the redox reaction with $NaBH_4$ and CuO, as previously discussed. According to Table 2, CeO_2-B prepared by chemical redox etching with $NaBH_4$ possessed the highest $[Ce^{3+}]$ and $[O_v]$ defect sites.

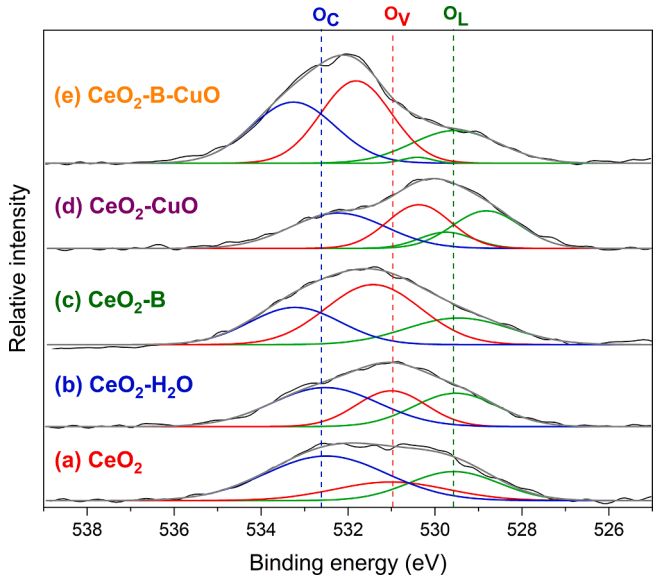

Fig. 8. XPS spectra of O 1 s of CeO_2 and surface modified CeO_2.

Table 2
The concentration fraction of Ce^{3+}, Ce^{4+} and O_V of CeO_2 and surface modified CeO_2.

Catalyst	[Ce^{4+}] (%)	[Ce^{3+}] (%)	[Ce^{3+}/Ce^{4+}] (%)	[O_v] (%)
CeO_2	90.94	9.06	9.97	20.81
CeO_2-H_2O	90.39	9.61	10.63	26.37
CeO_2-B	85.97	14.03	16.32	48.70
CeO_2-CuO	89.84	10.16	11.31	29.30
CeO_2-B-CuO	89.29	10.71	11.99	41.74

The increase of [O_v] of CeO_2-B catalyst suggested the relation between the B- species and the oxygen vacancy defects [66] in which the increase of O_V concentration might have been related to the formation of active oxygen (O^{2-}) caused by the reaction of borate (BO^{2-}) species as shown in Eqs. (10) and (11) [66,95]. In these reactions, sodium metaborate ($NaBO_2$) could have formed through the hydrolysis of $NaBH_4$ to create the BO^{2-} species. Subsequently, the BO^{2-} species reacted with the absorbed peroxide species (O_2^{2-}) on the surface of CeO_2. The reaction between BO^{2-} and O_2^{2-} was not only consuming the inactive peroxide species, but also enhancing the active oxygen (O^{2-}) on the surface of CeO_2-B and CeO_2-B-CuO catalysts [66,95]. This observation agreed well with the intensity reduction of the Raman active band of peroxide species after the surface modification as shown in Fig. 5. As the exposed Ce^{3+} coupled with oxygen vacancies on surface of CeO_2 catalysts were reported to be the active sites for the direct synthesis of DMC from CO_2 and methanol [52,57,95], modification of the CeO_2 surface with the $NaBH_4$ redox etching under a high intensity ultrasonication appeared to be an effective method to engineer the surface characteristics and possibly improve the catalytic activities of CeO_2 catalysts.

$$NaBH_4 + 2H_2O \rightarrow NaBO_2 + 4H_2 \quad (10)$$

$$BO_2^- + O_2^{2-} \rightarrow BO_3^- + O^{2-} \quad (11)$$

The NH_3 and CO_2 adsorption were examined to investigate the acid-base properties of the CeO_2 and surface modified CeO_2 nanospindle catalysts. Fig. 9 (a) and (b) show the NH_3 and CO_2-TPD profiles of all catalysts from 50 to 950 °C, respectively. The weak, moderate, and strong acid and basic sites were evaluated from the NH_3 and CO_2-TPD desorption peak areas at $<$ 200 °C, 200–400 °C and $>$ 400 °C, respectively [6–8]. The acidity and basicity of all catalysts are summarized in Table 3. CeO_2 and surface modified CeO_2 nanospindle catalysts can behave as bi-functional acid-base catalysts since their surface consists of both acidic and basic sites [7], which are required for the conversion of CO_2 and methanol to DMC [6–8]. The total acidity of CeO_2 nanospindles was 1.542 mmol.g^{-1} while the total basicity was 0.474 mmol.g^{-1}. After the surface modification, the total acidity and basicity were found to have decreased to 0.739–0.905 mmol.g^{-1} and 0.241–0.369 mmol.g^{-1}, respectively. Notable, the total acidity and basicity obtained in this study were comparable to those reported in the literature, in which the reported acidity and basicity values of CeO_2 catalysts varied between 0.25 and 0.63 and 0.08–0.73 mmol/g, respectively [8,17,103,105,106]. The decrease of acid and basic sites after the surface modification was inconsistent with the increase of surface oxygen vacancy concentration that was observed from other characterization techniques. Generally, oxygen vacancies serve as the Lewis acid sites on the CeO_2 surface, and the formation of oxygen vacancies consequently creates low coordinated oxygen anions which typically act as the Lewis basic sites [7,43]. The variation in acid-base properties observed in this study may have occurred due to the complex interaction of different types of surfaces species i.e., Ce^{4+}/Ce^{3+}, oxygen, B- and Cu- species with the surface adsorbates [8,103,105,106].

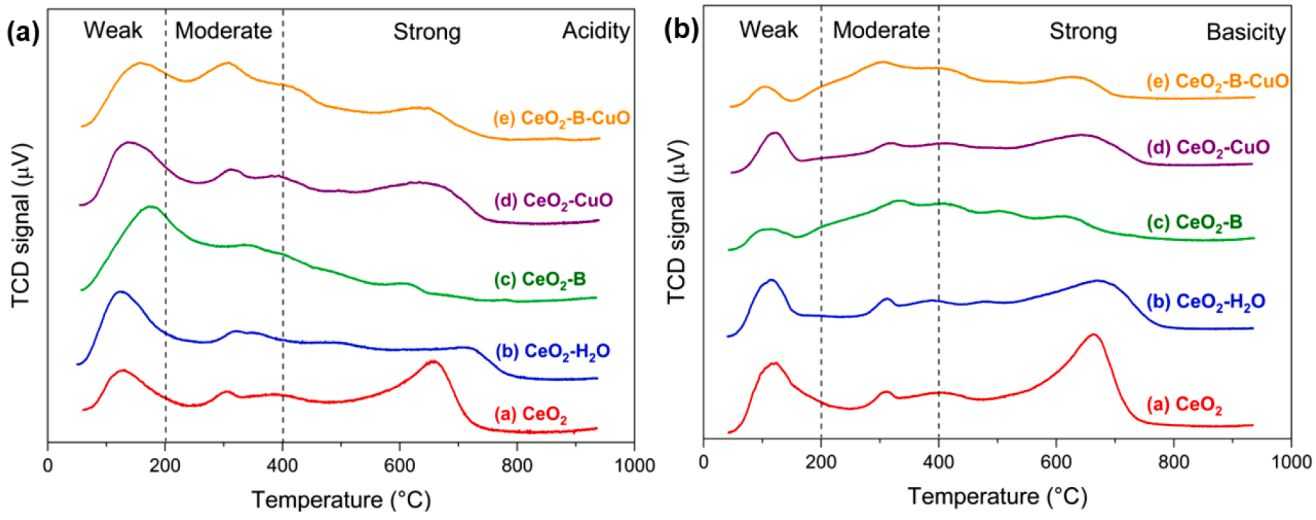

Fig. 9. TPD of (a) NH_3 and (b) CO_2-TPD profiles of CeO_2 and surface modified CeO_2.

Table 3
Acidic and basic values of all catalysts determined from NH_3 and CO_2-TPD measurements.

Catalyst	Acidity (mmol.g^{-1}; NH_3-TPD)				Basicity (mmol.g^{-1}; CO_2-TPD)			
	Weak (<200 °C)	Medium (200–400 °C)	Strong (>400 °C)	Total	Weak (<200 °C)	Medium (200–400 °C)	Strong (>400 °C)	Total
CeO_2	0.424	0.467	0.651	1.542	0.127	0.040	0.307	0.474
CeO_2-H_2O	0.364	0.190	0.331	0.885	0.092	0.081	0.196	0.369
CeO_2-B	0.372	0.227	0.140	0.739	0.025	0.109	0.176	0.310
CeO_2-CuO	0.301	0.278	0.273	0.852	0.038	0.101	0.117	0.256
CeO_2-B-CuO	0.278	0.415	0.212	0.905	0.017	0.152	0.072	0.241

3.2. Catalytic activity

Catalytic activity tests for the direct synthesis of DMC from CO_2 and methanol were performed over the CeO_2 and surface modified CeO_2 nanospindle catalysts. The DMC yield, methanol conversion, TOF and DMC selectivity are presented in Table 4 and Fig. 10. The catalytic activity tests showed that CeO_2 nanospindles that had been simply prepared by a precipitation method could catalyze the direct synthesis of DMC from CO_2 and methanol by providing high DMC yield at 14.44 mmol.g_{cat}^{-1}, methanol conversion at 0.29 %, TOF at 0.43 h^{-1} and 100 % DMC selectivity with only DMC, the remaining methanol, and by-product water contained in the liquid products. It should be noted that the % methanol conversion reported in this study was relatively low, which was because a high quantity of methanol feedstock at 40 ml was used in the reaction. After the surface modification, all catalysts showed higher performances than did the unmodified CeO_2, and the order of performance was CeO_2-B > CeO_2-B-CuO > CeO_2-CuO > CeO_2-H_2O > CeO_2. The DMC yield of CeO_2-H_2O was higher than the unmodified CeO_2, at 15.45 mmol.g_{cat}^{-1}, indicating that just the irradiation of the surface of CeO_2 nanospindles with a high intensity ultrasonic wave in deionized-water was able to increase the surface-active sites and consequently enhance the catalytic activity [107]. Among the surface modified catalysts, CeO_2-B exhibited the highest DMC yield at 17.90 mmol.g_{cat}^{-1}, 0.36 % methanol conversion, and TOF at 0.54 h^{-1}. The improvement of catalytic performance of CeO_2-B correlated with the rise of the concentration fraction of surface-active sites of exposed Ce^{3+} and oxygen vacancies caused by the chemical redox etching with $NaBH_4$ under high intensity ultrasonication [66]. The increase of surface Ce^{3+} and oxygen vacancies has been said to promote CO_2 and methanol adsorption, which are responsible for the increase of DMC yield formation [103]. The DMC yields of CeO_2-CuO (15.80 mmol.g_{cat}^{-1}) and CeO_2-B-CuO (16.47 mmol.g_{cat}^{-1}) were lower than that of CeO_2-B, but still higher than those of the unmodified CeO_2 and CeO_2-H_2O. This showed that the dispersion of nanocrystalline CuO on the CeO_2 surface was able to improve the catalytic activity due to the interaction between Cu ions and Ce ions and the formation of surface defect sites through the oxidation–reduction reaction of $Cu^{+} + Ce^{4+} \leftrightarrow Cu^{2+} + Ce^{3+}$ [31,52,58]. However, the effect of CuO on the improvement of catalytic activity of CeO_2 was lower when compared to that resulting from the chemical redox etching with $NaBH_4$. In case of CeO_2-B-CuO, treating the CeO_2 surface with $NaBH_4$ before impregnating with CuO led to strong interfacial bonding between the surface defect sites and the CuO species, which resulted in the reduction of surface-active area and did not enhance the DMC formation as much as expected.

The mechanism for DMC formation from CO_2 and methanol over the CeO_2-B catalyst is shown in Fig. 11. Firstly, a CeO_2-B catalyst was prepared by surface modification of CeO_2 nanospindles with a strong reducing agent, $NaBH_4$, under a high intensity ultrasonic irradiation in order to create surface-active sites of exposed Ce^{3+} and oxygen vacancies that could serve as Lewis acid sites [66,78,103]. The DMC formation began when CO_2 molecules were adsorbed onto the CeO_2-B surface through the Lewis acid-base interaction of oxygen vacancies on the catalyst surface and nonbonding electrons in the oxygen atoms of CO_2 [103,106]. Then, methanol molecules were adsorbed onto adjacent Ce^{3+} Lewis acid sites through the oxygen atoms of CH_3OH to form intermediate methoxy carbonyl ions ($CH_3OCO_2^-$). After that, other methanol molecules were absorbed on the opposite Ce^{3+} sites [43]. Next, H atoms from methanol molecules and O atoms in CO_2 molecules were removed through the Lewis acid-base reaction to create DMC and water by-product. Finally, oxygen vacancies were released onto the catalyst surface [106].

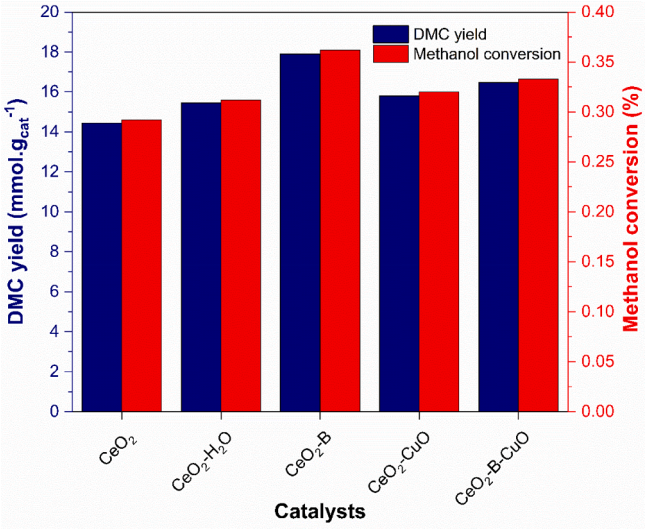

Fig. 10. Correlation between DMC yield and methanol conversion of CeO_2 and surface modified CeO_2.

Table 5 presents a comparison of the catalytic performance of CeO_2-based catalysts for the direct synthesis of DMC from CO_2 and methanol which involved similar systems to the ones used in this study. The surface modified CeO_2-B nanospindle catalysts prepared in this study showed higher DMC yields than those previously reported. These results suggested that chemical treatment of CeO_2 nanospindle surface with a redox etching reagent, $NaBH_4$, under a high intensity ultrasonication

Table 4
Catalytic activity of CeO_2 and surface modified CeO_2.

Catalyst	DMC yield (mmol)	DMC yield (mmol.g_{cat}^{-1})	Methanol Conversion (%)	TOF (h^{-1})	DMC selectivity (%)
CeO_2	1.44	14.44	0.29	0.43	100
CeO_2-H_2O	1.54	15.45	0.31	0.46	100
CeO_2-B	1.79	17.90	0.36	0.54	100
CeO_2-CuO	1.58	15.80	0.32	0.47	100
CeO_2-B-CuO	1.65	16.47	0.33	0.49	100

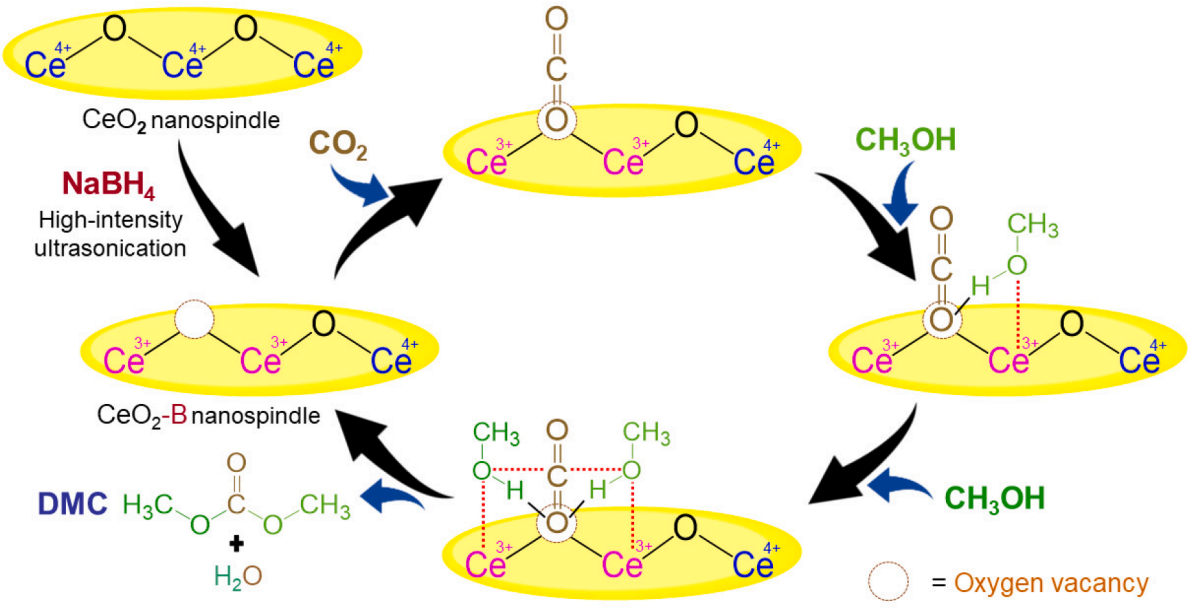

Fig. 11. Catalytic mechanism for the direct synthesis of DMC from CO_2 and methanol over CeO_2-B catalyst.

Table 5
Catalytic conversion of DMC from CO_2 and methanol using CeO_2 and surface modified CeO_2 catalysts.

Catalysts	Method		Morphology	Operation condition			DMC yield (mmol.g_{cat}^{-1})	Ref.
	Preparation	Modification		Cat. wt. (g)	Pressure (MPa)	Temp. (°C)		
CeO_2	Hydrothermal	–	Spindle	0.1	5.0	140	1.38	[17]
CeO_2	Precipitation	–	Spindle	1.0	8.0	140	13.84	[43]
CeO_2	Hydrothermal	–	Rod	0.2	3.0	160	0.20	[44]
CeO_2	Solvothermal	Thermal reduction under H_2	Wire	0.2	5.0	120	16.85	[35]
CuO/CeO_2	Hydrothermal	Impregnation	Rod	0.5	3.0	140	0.60	[70]
CeO_2	Precipitation	–	Spindle	0.1	4.5	140	14.44	This work
CeO_2-B	Precipitation	Chemical redox etching	Spindle	0.1	4.5	140	17.90	This work
CeO_2-B-CuO	Precipitation	Chemical redox etching & Impregnation	Spindle	0.1	4.5	140	16.47	This work

was a simple and effective method to enhance the catalytic activity of CeO_2 nanospindles for the production of DMC.

4. Conclusion

In this study, we reported a simple and effective method that can be used to modify the surface properties of CeO_2 nanospindles via an ultrasonically assisted wet chemical redox etching. The CeO_2 nanospindles were first prepared via a precipitation method, and this was followed by chemical treatment with a strong reducing agent, $NaBH_4$, and/or Cu solution under high intensity ultrasonic irradiation. The particle collisions and surface reduction induced by the sonochemical effect and redox reaction resulted in an increase of surface-active sites of exposed Ce^{3+} and oxygen vacancies. CeO_2-B showed the highest catalytic activity for the conversion of CO_2 and methanol to DMC, which corresponded well with the increased number of surface-active sites capable of absorbing reactant species and subsequently participating in the formation reaction. These results suggest that the ultrasonically assisted wet chemical redox etching is a simple and effective method to engineer the surface properties of CeO_2 catalysts.

Declaration of Competing Interest

The authors declare that they have no known competing financial interests or personal relationships that could have appeared to influence the work reported in this paper.

Data availability

Data will be made available on request.

Acknowledgements

This project is funded by National Research Council of Thailand (NRCT) and King Mongkut's Institute of Technology Ladkrabang : N42A650388. We thank J. Duagtanon, C. Sreemueang, P. Noppharat and C. Muangsuwan for laboratory assistance and the Scientific Instruments Center, Faculty of Science, King Mongkut's Institute of Technology Ladkrabang.

References

[1] K.M.D.B. Baojuan Zhenga, B.C. Owsley, G.M. Henebry, Scaling relationship between CO pollution and population size over major US metropolitan statistical areas, Landscape Urban Plann. 187 (2019) 191–198.
[2] R. Saada, S. Kellici, T. Heil, D. Morgan, B. Saha, Greener synthesis of dimethyl carbonate using a novel ceria-zirconia oxide/graphene nanocomposite catalyst, Appl. Catal. B Environ. 168–169 (2015) 353–362.
[3] G.P. Peters, C. Le Quéré, R.M. Andrew, J.G. Canadell, P. Friedlingstein, T. Ilyina, R.B. Jackson, F. Joos, J.I. Korsbakken, G.A. McKinley, S. Sitch, P. Tans, Towards real-time verification of CO_2 emissions, Nature Clim. Change 7 (2017) 848–850.
[4] A.A. Marciniak, O.C. Alves, L.G. Appel, C.J.A. Mota, Synthesis of dimethyl carbonate from CO_2 and methanol over CeO_2: Role of copper as dopant and the use of methyl trichloroacetate as dehydrating agent, J. Catal. 371 (2019) 88–95.
[5] P. Friedlingstein, R.M. Andrew, J. Rogelj, G.P. Peters, J.G. Canadell, R. Knutti, G. Luderer, M.R. Raupach, M. Schaeffer, D.P. van Vuuren, C. Le Quéré, Persistent

growth of CO_2 emissions and implications for reaching climate targets, Nat. Geosci. 7 (2014) 709–715.
[6] P. Kumar, P. With, V.C. Srivastava, R. Gläser, I.M. Mishra, Conversion of carbon dioxide along with methanol to dimethyl carbonate over ceria catalyst, J. Environ. Chem. Eng. 3 (2015) 2943–2947.
[7] P. Kumar, V.C. Srivastava, R. Gläser, P. With, I.M. Mishra, Active ceria-calcium oxide catalysts for dimethyl carbonate synthesis by conversion of CO_2, Powder Technol. 309 (2017) 13–21.
[8] U. P, S. Darbha,, Direct synthesis of dimethyl carbonate from CO_2 and methanol over CeO_2 catalysts of different morphologies, J. Chem. Sci. 128 (2016) 957–965.
[9] M. Zhang, Y. Xu, B.L. Williams, M. Xiao, S. Wang, D. Han, L. Sun, Y. Meng, Catalytic materials for direct synthesis of dimethyl carbonate (DMC) from CO_2, J. Cleaner Prod. 279 (2021).
[10] G. Centi, S. Perathoner, Opportunities and prospects in the chemical recycling of carbon dioxide to fuels, Catal. Today 148 (2009) 191–205.
[11] G.A. Olah, Chemical recycling of carbon dioxide to methanol and dimethyl ether: From greenhouse gas to renewable, environmentally carbon neutral fuels and synthetic hydrocarbons, J. Org. Chem. 74 (2009) 487–498.
[12] B. Hu, C. Guild, S.L. Suib, Thermal, electrochemical, and photochemical conversion of CO_2 to fuels and value-added products, J. CO_2 Utiliz. 1 (2013) 18–27.
[13] X. Frogneux, O. Jacquet, T. Cantat, Iron-catalyzed hydrosilylation of CO_2: CO_2 conversion to formamides and methylamines, Catal. Sci. Technol. 4 (2014) 1529–1533.
[14] B.A.V. Santos, V.M.T.M. Silva, J.M. Loureiro, A.E. Rodrigues, Review for the direct synthesis of dimethyl carbonate, ChemBioEng Rev. 1 (2014) 214–229.
[15] H. J. Kuenen, H. J. Mengers, A. G. J. van der Ham , A. A. Kiss, Novel process for conversion of CO_2 to dimethyl carbonate using catalytic membrane reactors, in: 26th European Symposium on Computer Aided Process Engineering, 2016, pp. 991-996.
[16] A.A. Marciniak, F.J.F.S. Henrique, A.F.F. de Lima, O.C. Alves, C.R. Moreira, L. G. Appel, C.J.A. Mota, What are the preferred CeO_2 exposed planes for the synthesis of dimethyl carbonate? Answers from theory and experiments, Mol. Catal. 493 (2020).
[17] S. Wang, L. Zhao, W. Wang, Y. Zhao, G. Zhang, X. Ma, J. Gong, Morphology control of ceria nanocrystals for catalytic conversion of CO_2 with methanol, Nanoscale 5 (2013) 5582–5588.
[18] B. Schäffner,, Organic carbonates as solvents in synthesis and catalysis, Chem. Rev. 110 (2010) 4554–4581.
[19] Y. Yoshida, Y. Arai, S. Kado, K. Kunimori, K. Tomishige, Direct synthesis of organic carbonates from the reaction of CO_2 with methanol and ethanol over CeO_2 catalysts, Catal. Today 115 (2006) 95–101.
[20] B. Newman, t-Carbinamines, RR'R''CNH2. 111. The preparation of isocyanates, isothiocyanates and related compounds, Contribution from the Rohm & Haas company, 123 (1956) 358-4361.
[21] S. Maurizio, The addition reduction of dlalkyl carbonate to ketones, Gazz. Chim. Ital. 123 (1993) 515–518.
[22] V. Isabelle, An environmentally benign access to carbamates and ureas, Tetrahedron Lett. 41 (2000) 6347–6350.
[23] S. Maurizio, The synthesis of alkyl carbamates from primary aliphatic amines and dialkyl carbonates in supercritical carbon dioxide, Tetrahedron Lett. 43 (2002) 1217–1219.
[24] D. Delledonne, Developments in the production and application of dimethylcarbonate, Appl. Catal. A 221 (2001) 241–251.
[25] B. Harry, The chemistry of phosgene, Chem. Rev. 73 (1973) 75–91.
[26] R. Ugo, Synthesis of dimethyl carbonate from methanol, carbon monoxide, and oxygen catalyzed by copper compounds, Ind. Eng. Chem. Prod. Res. Dev. 19 (1980) 396–403.
[27] S. King, Oxidative carbonylation of methanol to dimethyl carbonate by solid-state ion-exchanged CuY catalysts, Catal. Today 33 (1997) 173–182.
[28] P. W. J., Preparation and properties of the alkylene carbonates, Ind. Eng. Chem. 50 (1958) 767–770.
[29] H. Cui, T. Wang, F. Wang, C. Gu, P. Wang, Y. Dai, Transesterification of ethylene carbonate with methanol in supercritical carbon dioxide, J. Supercrit. Fluids 30 (2004) 63–69.
[30] Q. Liu, L. Wu, R. Jackstell, M. Beller, Using carbon dioxide as a building block in organic synthesis, Nat. Commun. 6 (2015) 5933.
[31] J. Bian, X.W. Wei, Y.R. Jin, L. Wang, D.C. Luan, Z.P. Guan, Direct synthesis of dimethyl carbonate over activated carbon supported Cu-based catalysts, Chem. Eng. J. 165 (2010) 686–692.
[32] Y. Cao, H. Cheng, L. Ma, F. Liu, Z. Liu, Research progress in the direct synthesis of dimethyl carbonate from CO_2 and methanol, Catal. Surv. Asia 16 (2012) 138–147.
[33] M. Aresta, A. Dibenedetto, A. Dutta, Energy issues in the utilization of CO_2 in the synthesis of chemicals: the case of the direct carboxylation of alcohols to dialkyl-carbonates, Catal. Today 281 (2017) 345–351.
[34] A.H. Tamboli, A.A. Chaugule, H. Kim, Catalytic developments in the direct dimethyl carbonate synthesis from carbon dioxide and methanol, Chem. Eng. J. 323 (2017) 530–544.
[35] Z. Fu, Y. Yu, Z. Li, D. Han, S. Wang, M. Xiao, Y. Meng, Surface reduced CeO_2 nanowires for direct conversion of CO_2 and methanol to dimethyl carbonate: catalytic performance and role of oxygen vacancy, Catalysts 8 (2018).
[36] S. Fang, Direct synthesis of dimethyl carbonate from carbon dioxide and methanol catalyzed by base, Appl. Catal. A 142 (1996) L1–L3.
[37] Q. Yang, H. Wang, X. Ding, X. Yang, Y. Wang, One-pot synthesis of dimethyl carbonate from carbon dioxide, cyclohexene oxide, and methanol, Res. Chem. Intermed. 41 (2013) 4101–4111.
[38] K.T. Jung, A.T. Bell, An in situ infrared study of dimethyl carbonate synthesis from carbon dioxide and methanol over zirconia, J. Catal. 204 (2001) 339–347.
[39] K.T. Jung, Effects of catalyst phase structure on the elementary processes involved in the synthesis of dimethyl carbonate from methanol and carbon dioxide over zirconia, Top. Catal. 20 (2002) 97–105.
[40] X. Chen, L. Liu, P.Y. Yu, S.S. Mao, Increasing solar absorption for photocatalysis with black hydrogenated titanium dioxide nanocrystals, Science 331 (2011) 746–750.
[41] M. Ge, C. Cao, J. Huang, S. Li, Z. Chen, K.-Q. Zhang, S.S. Al-Deyab, Y. Lai, A review of one-dimensional TiO_2 nanostructured materials for environmental and energy applications, J. Mater. Chem. A 4 (2016) 6772–6801.
[42] M. Honda, A. Suzuki, B. Noorjahan, K. Fujimoto, K. Suzuki, K. Tomishige, Low pressure CO_2 to dimethyl carbonate by the reaction with methanol promoted by acetonitrile hydration, Chem. Commun. (Camb.) 4596–8 (2009).
[43] A.H. Tamboli, N. Suzuki, C. Terashima, S. Gosavi, H. Kim, A. Fujishima, Direct dimethyl carbonates synthesis over CeO_2 and evaluation of catalyst morphology role in catalytic performance, Catalysts 11 (2021).
[44] M. Luo, T. Qin, Q. Liu, Z. Yang, F. Wang, H. Li, Novel Fe-modified CeO_2 nanorod catalyst for the dimethyl carbonate formation from CO_2 and methanol, ChemCatChem 14 (2022).
[45] K. Saravanakumar, M.M. Ramjan, P. Suresh, V. Muthuraj, Fabrication of highly efficient visible light driven Ag/CeO_2 photocatalyst for degradation of organic pollutants, J. Alloy. Compd. 664 (2016) 149–160.
[46] R. Bakkiyaraj, M. Balakrishnan, G. Bharath, N. Ponpandian, Facile synthesis, structural characterization, photocatalytic and antimicrobial activities of Zr doped CeO_2 nanoparticles, J. Alloy. Compd. 724 (2017) 555–564.
[47] Y. Qi, J. Ye, S. Zhang, Q. Tian, N. Xu, P. Tian, G. Ning, Controllable synthesis of transition metal ion-doped CeO_2 micro/nanostructures for improving photocatalytic performance, J. Alloy. Compd. 782 (2019) 780–788.
[48] D. Zhang, X. Du, L. Shi, R. Gao, Shape-controlled synthesis and catalytic application of ceria nanomaterials, Dalton Trans. 41 (2012) 14455–14475.
[49] C. Sun, H. Li, L. Chen, Nanostructured ceria-based materials: synthesis, properties, and applications, Energy Environ. Sci. 5 (2012).
[50] L. Vivier, D. Duprez, Ceria-based solid catalysts for organic chemistry, ChemSusChem 3 (2010) 654–678.
[51] C.T. Campbell, C.H. Peden, Oxygen vacancies and catalysis on ceria surfaces, Science 309 (2005) 713–714.
[52] X. Zhang, L. Su, Y. Kong, D. Ma, Y. Ran, S. Peng, L. Wang, Y. Wang, CeO_2 nanoparticles modified by CuO nanoparticles for low-temperature CO oxidation with high catalytic activity, J. Phys. Chem. Solids 147 (2020).
[53] N.V. Skorodumova, M. Baudin, K. Hermansson, Surface properties of CeO_2 from first principles, Phys. Rev. B 69 (2004).
[54] K. Zhou, X. Wang, X. Sun, Q. Peng, Y. Li, Enhanced catalytic activity of ceria nanorods from well-defined reactive crystal planes, J. Catal. 229 (2005) 206–212.
[55] R. Si, M. Flytzani-Stephanopoulos, Shape and crystal-plane effects of nanoscale ceria on the activity of Au-CeO_2 catalysts for the water-gas shift reaction, Angew. Chem. Int. Ed. Engl. 47 (2008) 2884–2887.
[56] L. Chen, S. Wang, J. Zhou, Y. Shen, Y. Zhao, X. Ma, Dimethyl carbonate synthesis from carbon dioxide and methanol over CeO_2 versus over ZrO_2: comparison of mechanisms, RSC Adv. 4 (2014) 30968–30975.
[57] J. Chen, Y. Wanyan, J. Zeng, H. Fang, Z. Li, Y. Dong, R. Qin, C. Wu, D. Liu, M. Wang, Q. Kuang, Z. Xie, L. Zheng, Surface engineering protocol to obtain an atomically dispersed Pt/CeO_2 catalyst with high activity and stability for CO oxidation, ACS Sustain. Chem. Eng. 6 (2018) 14054–14062.
[58] S. Wada, K. Oka, K. Watanabe, Y. Izumi, Catalytic conversion of carbon dioxide into dimethyl carbonate using reduced copper-cerium oxide catalysts as low as 353 K and 1.3 MPa and the reaction mechanism, Front. Chem. 1 (2013) 8.
[59] Y. Ma, W. Gao, Z. Zhang, S. Zhang, Z. Tian, Y. Liu, J.C. Ho, Y. Qu, Regulating the surface of nanoceria and its applications in heterogeneous catalysis, Surf. Sci. Rep. 73 (2018) 1–36.
[60] E. Mamontov, Lattice defects and oxygen storage capacity of nanocrystalline ceria and ceria-zirconia, J. Phys. Chem. B 104 (2000) 11110–11116.
[61] S. Nader, Reduced erbium-doped ceria nanoparticles: one nano-host applicable for simultaneous optical down- and up-conversions, Nanoscale Res. Lett. 9 (2014) 1–6.
[62] N.J. Lawrence, J.R. Brewer, L. Wang, T.S. Wu, J. Wells-Kingsbury, M.M. Ihrig, G. Wang, Y.L. Soo, W.N. Mei, C.L. Cheung, Defect engineering in cubic cerium oxide nanostructures for catalytic oxidation, Nano Lett. 11 (2011) 2666–2671.
[63] T.S. Sakthivel, D.L. Reid, U.M. Bhatta, G. Mobus, D.C. Sayle, S. Seal, Engineering of nanoscale defect patterns in CeO_2 nanorods via ex situ and in situ annealing, Nanoscale 7 (2015) 5169–5177.
[64] M.M. Khan, S.A. Ansari, D. Pradhan, D.H. Han, J. Lee, M.H. Cho, Defect-induced band gap narrowed CeO_2 nanostructures for visible light activities, Ind. Eng. Chem. Res. 53 (2014) 9754–9763.
[65] J. Li, Z. Zhang, W. Gao, S. Zhang, Y. Ma, Y. Qu, Pressure regulations on the surface properties of CeO_2 nanorods and their catalytic activity for CO oxidation and nitrile hydrolysis reactions, ACS Appl. Mater. Interfaces 8 (2016) 22988–22996.
[66] Y. Wang, Z. Liu, R. Wang, $NaBH_4$ surface modification on CeO_2 nanorods supported transition-metal catalysts for low temperature CO oxidation, ChemCatChem 12 (2020) 4304–4316.

[67] W. Gao, Z. Zhang, J. Li, Y. Ma, Y. Qu, Surface engineering on CeO_2 nanorods by chemical redox etching and their enhanced catalytic activity for CO oxidation, Nanoscale 7 (2015) 11686–11691.

[68] Y. Wang, R. Wang, Effects of chemical etching and reduction activation of CeO_2 nanorods supported ruthenium catalysts on CO oxidation, J. Colloid Interface Sci. 613 (2022) 836–846.

[69] Z. Wei, R. Wang, Chemically etched CeO_{2-x} nanorods with abundant surface defects as effective cathode additive for trapping lithium polysulfides in Li-S batteries, J. Colloid Interface Sci. 615 (2022) 527–542.

[70] J. Al-Darwish, M. Senter, S. Lawson, F. Rezaei, A.A. Rownaghi, Ceria nanostructured catalysts for conversion of methanol and carbon dioxide to dimethyl carbonate, Catal. Today 350 (2020) 120–126.

[71] P. Seeharaj, P. Kongmun, P. Paiplod, S. Prakobmit, C. Sriwong, P. Kim-Lohsoontorn, N. Vittayakorn, Ultrasonically-assisted surface modified TiO_2/rGO/CeO_2 heterojunction photocatalysts for conversion of CO_2 to methanol and ethanol, Ultrason. Sonochem. 58 (2019), 104657.

[72] E. Thasirisap, N. Vittayakorn, P. Seeharaj, Surface modification of TiO_2 particles with the sono-assisted exfoliation method, Ultrason. Sonochem. 39 (2017) 733–740.

[73] P. Pasupong, K. Choojun, N. Vittayakorn, P. Seeharaj, Synthesis of nanocrystalline cobalt ferrite by the sonochemical method in highly basic aqueous solution, Key Eng. Mater. 751 (2017) 368–373.

[74] P. Seeharaj, T. Charoonsuk, P. Pasupong, P. Kim-Lohsoontorn, N. Vittayakorn, Phase formation, microstructure, and densification of Yttrium-doped Barium Zirconate prepared by the sonochemical method, Int. J. Appl. Ceram. Technol. 13 (2016) 200–208.

[75] P. Kumar, L. Matoh, R. Kaur, U.L. Štangar, Synergic effect of manganese oxide on ceria based catalyst for direct conversion of CO_2 to green fuel additive: catalyst activity and thermodynamics study, Fuel 285 (2021).

[76] D.J. Faria, L. Moreira Dos Santos, F.L. Bernard, I. Selbacch Pinto, M.A. Carmona da Motta Resende, S. Einloft, Dehydrating agent effect on the synthesis of dimethyl carbonate (DMC) directly from methanol and carbon dioxide, RSC Adv. 10 (2020) 34895–34902.

[77] M. Liu, M. Konstantinova, L. Negahdar, J. McGregor, The role of Zn in the sustainable one-pot synthesis of dimethyl carbonate from carbon dioxide, methanol and propylene oxide, Chem. Eng. Sci. 231 (2021).

[78] H. Kim, K. Suslick, The effects of ultrasound on crystals: sonocrystallization and sonofragmentation, Crystals 8 (2018).

[79] C. Ruirun, Z. Deshuang, M. Tengfei, D. Hongsheng, S. Yanqing, G. Jingjie, F. Hengzhi, Effects of ultrasonic vibration on the microstructure and mechanical properties of high alloying TiAl, Sci. Rep. 7 (2017) 41463.

[80] Z. Zhang, D.-W. Sun, Z. Zhu, L. Cheng, Enhancement of crystallization processes by power ultrasound: current state-of-the-art and research advances, Compr. Rev. Food Sci. Food Saf. 14 (2015) 303–316.

[81] A.D. Liyanage, S.D. Perera, K. Tan, Y. Chabal, K.J. Balkus, Synthesis, characterization, and photocatalytic activity of Y-doped CeO_2 nanorods, ACS Catal. 4 (2014) 577–584.

[82] P. Kim-Lohsoontorn, V. Tiyapongpattana, N. Asarasri, P. Seeharaj, N. Laosiripojana, Preparation of CeO_2 nano rods through a sonication-assisted precipitation, Int. J. Appl. Ceram. Technol. 11 (2014) 645–653.

[83] X. Liu, J. Ding, X. Lin, R. Gao, Z. Li, W.-L. Dai, Zr-doped CeO_2 nanorods as versatile catalyst in the epoxidation of styrene with tert-butyl hydroperoxide as the oxidant, Appl. Catal. A 503 (2015) 117–123.

[84] M.E. Culica, A.L. Chibac-Scutaru, V. Melinte, S. Coseri, Cellulose acetate incorporating organically functionalized CeO_2 NPs: efficient materials for UV filtering applications, Materials (Basel) 13 (2020).

[85] G. Jayakumar, A.A. Irudayaraj, A.D. Raj, Investigation on the synthesis and photocatalytic activity of activated carbon–cerium oxide (AC–CeO_2) nanocomposite, Appl. Phys. A 125 (2019).

[86] M. Jobbágy, F. Mariño, B. Schönbrod, G. Baronetti, M. Laborde, Synthesis of copper-promoted CeO_2 catalysts, Chem. Mater. 18 (2006) 1945–1950.

[87] M. Farahmandjou, Synthesis of cerium oxide (CeO_2) nanoparticles using simple CO-precipitation method, Rev. Mexi. Física 62 (2016) 496–499.

[88] N. Ramjeyanthi, Effect of calcination temperature on the structural and optical properties of synthesized CeO_2 nanoparticles via chemical method, J. Appl. Sci. Comput. 5 (2018) 577–583.

[89] S. Phoka, P. Laokul, E. Swatsitang, V. Promarak, S. Seraphin, S. Maensiri, Synthesis, structural and optical properties of CeO_2 nanoparticles synthesized by a simple polyvinyl pyrrolidone (PVP) solution route, Mater. Chem. Phys. 115 (2009) 423–428.

[90] E. Kumar, P. Selvarajan, D. Muthuraj, Synthesis and characterization of CeO_2 nanocrystals by solvothermal route, Mater. Res. 16 (2013) 269–276.

[91] T.T. Le, C. Pistidda, J. Puszkiel, C. Milanese, S. Garroni, T. Emmler, G. Capurso, G. Gizer, T. Klassen, M. Dornheim, Efficient synthesis of alkali borohydrides from mechanochemical reduction of borates using magnesium–aluminum-based waste, Metals 9 (2019).

[92] J. Andrieux, C. Goutaudier, L. Laversenne, E. Jeanneau, P. Miele, Synthesis, characterization, and crystal structure of a new trisodium triborate, $Na_3[B_3O_4(OH)_4]$, Inorg. Chem. 49 (2010) 4830–4835.

[93] M.E. Kibar, A.N. Akin, A novel process for CO_2 capture by using sodium metaborate. Part I: effects of calcination, Environ. Sci. Pollut. Res. Int. 25 (2018) 3446–3457.

[94] L. Yin, Y. Wang, G. Pang, Y. Koltypin, A. Gedanken, Sonochemical synthesis of cerium oxide nanoparticles-effect of additives and quantum size effect, J. Colloid Interface Sci. 246 (2002) 78–84.

[95] M.S. İzgi, O. Baytar, Ö. Şahin, H.Ç. Kazıcı, CeO_2 supported multimetallic nano materials as an efficient catalyst for hydrogen generation from the hydrolysis of $NaBH_4$, Int. J. Hydrogen Energy 45 (2020) 34857–34866.

[96] H. Zhang, Y. Zhou, Y. Li, T.J. Bandosz, D.L. Akins, Synthesis of hollow ellipsoidal silica nanostructures using a wet-chemical etching approach, J. Colloid Interface Sci. 375 (2012) 106–111.

[97] M. Guo, J. Lu, Y. Wu, Y. Wang, M. Luo, UV and visible Raman studies of oxygen vacancies in rare-earth-doped ceria, Langmuir 27 (2011) 3872–3877.

[98] W.H. Weber, K.C. Hass, J.R. McBride, Raman study of CeO_2: second-order scattering, lattice dynamics, and particle-size effects, Phys. Rev. B: Condens. Matter 48 (1993) 178–185.

[99] Y. Su, S. Yuan, D. Ning, Q. Zhang, W. Han, Y. Wang, The template-free synthesis of CuO@CeO_2 nanospheres: facile strategy, structure optimization, and enhanced catalytic activity toward CO oxidation, Eur. J. Inorg. Chem. 2018 (2018) 2927–2934.

[100] A. Pilli, J. Jones, N. Chugh, J. Kelber, F. Pasquale, A. LaVoie, Atomic layer deposition of BN as a novel capping barrier for B_2O_3, J. Vac. Sci. Technol., A 37 (2019).

[101] Y. Wang, Y. Lü, W. Zhan, Z. Xie, Q. Kuang, L. Zheng, Synthesis of porous Cu_2O/CuO cages using Cu-based metal–organic frameworks as templates and their gas-sensing properties, J. Mater. Chem. A 3 (2015) 12796–12803.

[102] Z. Chen, C.X. Kronawitter, X. Yang, Y.W. Yeh, N. Yao, B.E. Koel, The promoting effect of tetravalent cerium on the oxygen evolution activity of copper oxide catalysts, PCCP 19 (2017) 31545–31552.

[103] B. Liu, C. Li, G. Zhang, X. Yao, S.S.C. Chuang, Z. Li, Oxygen vacancy promoting dimethyl carbonate synthesis from CO_2 and methanol over Zr-doped CeO_2 nanorods, ACS Catal. 8 (2018) 10446–10456.

[104] J. Hu, K. Shen, Z. Liang, J. Hu, H. Sun, H. Zhang, Q. Tian, P. Wang, Z. Jiang, H. Huang, F. Song, Revealing the adsorption and decomposition of EP-PTCDI on a cerium oxide surface, ACS Omega 4 (2019) 17939–17946.

[105] Z. Fu, Y. Zhong, Y. Yu, L. Long, M. Xiao, D. Han, S. Wang, Y. Meng, TiO_2-doped CeO_2 nanorod catalyst for direct conversion of CO_2 and CH_3OH to dimethyl carbonate: catalytic performance and kinetic study, ACS Omega 3 (2018) 198–207.

[106] B. Liu, C. Li, G. Zhang, L. Yan, Z. Li, Direct synthesis of dimethyl carbonate from CO_2 and methanol over CaO-CeO_2 catalysts: the role of acid–base properties and surface oxygen vacancies, New J. Chem. 41 (2017) 12231–12240.

[107] T. Alammar, H. Noei, Y. Wang, W. Grünert, A.-V. Mudring, Ionic liquid-assisted sonochemical preparation of CeO_2 nanoparticles for CO oxidation, ACS Sustain. Chem. Eng. 3 (2014) 42–54.